Nuclear Engineering and Design 308 (2016) 238–251

Contents lists available at ScienceDirect

Nuclear Engineering and Design

journal homepage: www.elsevier.com/locate/nucengdes

Application of FFTBM with signal mirroring to improve accuracy assessment of MELCOR code

Mahdi Saghafi [a], Mohammad Bagher Ghofrani [a,*], Francesco D'Auria [b]

[a] Department of Energy Engineering, Sharif University of Technology, Azadi Avenue, Tehran, Iran
[b] San Piero a Grado Nuclear Research Group (GRNSPG), University of Pisa, Via Livornese 1291, San Piero a Grado, Pisa, Italy

HIGHLIGHTS

- FFTBM-SM is an improved Fast Fourier Transform Base Method by signal mirroring.
- FFTBM-SM has been applied to accuracy assessment of MELCOR code predictions.
- The case studied was Station Black-Out accident in PSB-VVER integral test facility.
- FFTBM-SM eliminates fluctuations of accuracy indices when signals sharply change.
- Accuracy assessment is performed in a more realistic and consistent way by FFTBM-SM.

ARTICLE INFO

Article history:
Received 24 May 2016
Received in revised form 14 August 2016
Accepted 19 August 2016
Available online 17 September 2016

JEL classification:
K. Thermal Hydraulics

ABSTRACT

This paper deals with the application of Fast Fourier Transform Base Method (FFTBM) with signal mirroring (FFTBM-SM) to assess accuracy of MELCOR code. This provides deeper insights into how the accuracy of MELCOR code in predictions of thermal-hydraulic parameters varies during transients. The case studied was modeling of Station Black-Out (SBO) accident in PSB-VVER integral test facility by MELCOR code. The accuracy of this thermal-hydraulic modeling was previously quantified using original FFTBM in a few number of time-intervals, based on phenomenological windows of SBO accident. Accuracy indices calculated by original FFTBM in a series of time-intervals unreasonably fluctuate when the investigated signals sharply increase or decrease. In the current study, accuracy of MELCOR code is quantified using FFTBM-SM in a series of increasing time-intervals, and the results are compared to those with original FFTBM. Also, differences between the accuracy indices of original FFTBM and FFTBM-SM are investigated and correction factors calculated to eliminate unphysical effects in original FFTBM. The main findings are: (1) replacing limited number of phenomena-based time-intervals by a series of increasing time-intervals provides deeper insights about accuracy variation of the MELCOR calculations, and (2) application of FFTBM-SM for accuracy evaluation of the MELCOR predictions, provides more reliable results than original FFTBM by eliminating the fluctuations of accuracy indices when experimental signals sharply increase or decrease. These studies have been performed in the framework of a research project, aiming to develop an appropriate accident management support tool for Bushehr nuclear power plant.

1. Introduction

Reliable application of thermal-hydraulic (TH) codes for analysis of transients and accidents in Nuclear Power Plants (NPPs), necessitates to follow qualified procedures with specific criteria for accuracy assessment of the code predictions (Petruzzi and D'Auria, 2008). D'Auria et al. (1994) in University of Pisa, developed a suitable method for qualification of best-estimate TH codes. It consists of Fast Fourier Transform Base Method (FFTBM) to quantify the accuracy of TH codes using experimental tests performed on integral test facilities (ITFs). FFTBM provides an integral quantitative representation of the code accuracy, comparing the calculated and experimental time-trends in frequency domain. FFTBM is extensively used for assessment and validation of different TH codes such as RELAP5, CATHARE, ATHLET, TRAC, KORSAR and TECH (D'Auria et al., 2004; Del Nevo et al., 2012; Prošek et al., 2002).

Normally, accuracy assessment using FFTBM is performed in a few number of time-intervals which are based on the phenomenological windows of the accidents. Using a series of time-intervals to

* Corresponding author. Fax: +98 2166166102.
E-mail address: ghofrani@sharif.edu (M.B. Ghofrani).

http://dx.doi.org/10.1016/j.nucengdes.2016.08.025
0029-5493/

Nomenclature

$\Delta\tilde{F}$	error function amplitude
$\tilde{F}_{exp}$	time function amplitude
ΔF	error function
AA	average amplitude
AM	accident management
BRU-A	safety valve in steam line
EREC	Electrogorsk Research and Engineering Center
f	frequency
F	time function
FASIV	Fast Acting Steam Isolating Valves
FFTBM	Fast Fourier Transform Base Method
FFTBM-SM	FFTBM with signal mirroring
ITF	integral test facility
MCP	Main Coolant Pump
MELCOR	methods for estimation of leakages and consequences of releases
NPP	Nuclear Power Plant
N	number of analyzed variables
PORV	pressure Operated Relief Valve
PRZ	pressurizer
PSB-VVER	integral thermal-hydraulic test facility located at EREC
SBO	Station Black-Out
SG	steam generator
t	time
TH	thermal-hydraulic
UP	Upper Plenum
VVER	Voda-Vodianye Energeticheski Reaktoryi
W_f	weighting factor
WF	weighting frequency

Subscripts

calc	calculated
err	error function
exp	experimental
i	ith variable
m	calculated with symmetrized signals by signal mirroring
norm	normalized
saf	safety
tot	total
var	variable

Superscript

m	power of 2

perform accuracy assessments, presents a more complete image of the code accuracy. It is revealed that if FFTBM is used for accuracy assessment, especially with a series of time-intervals, the accuracy index unreasonably changes when experimental signals sharply increase or decrease (e.g. triangular shape) (Prošek et al., 2008). Difference between the first and last data points of the investigated signals leads to presence of an artificial edge in periodically extended signals when performing the discreet Fourier transform (Prošek and Leskovar, 2015). Accuracy assessment is thus affected by frequencies from such artificial edge. Hence, improved FFTBM with signal mirroring (FFTBM-SM) was presented by Prošek et al. (2008) to eliminate unphysical fluctuations of accuracy indices and to perform accuracy assessments in a consistent and reasonable way.

The purpose of the current study is to quantitatively assess the accuracy of the MELCOR calculations using FFTBM-SM. The case studied was modeling Station Black-Out (SBO) accident in PSB-VVER ITF. PSB-VVER is a large scale (1:300) ITF which has been widely used in validation of TH codes for VVER-1000 NPPs (Del Nevo et al., 2012; Groudev et al., 2005; Heralecky, 2014; Nevo et al., 2008). Quality assessment of TH codes for application in VVER-type NPPs, involves the availability of qualified nodalizations as well as experimental data (Bucalossi et al., 2012). A TH nodalization for modeling PSB-VVER ITF by MELCOR code was previously developed (Saghafi et al., 2016) in the framework of a research project, aiming to develop an appropriate accident management support tool for Bushehr NPP (Saghafi and Ghofrani, 2015). Capability of the developed nodalization to reproduce the ITF behavior was evaluated and qualified at both steady-state and transient levels. At the transient level, acceptability of the calculations was qualitatively and quantitatively assessed. Quantitative evaluation of the transient level was carried out using original FFTBM for 5 time-intervals defined by phenomenological windows of SBO accident. In this study, accuracy assessment of MELCOR code is carried out using original FFTBM and FFTBM-SM in a series of time-intervals. Also, differences between the accuracy indices of original FFTBM and FFTBM-SM are investigated and correction factors are calculated for original FFTBM to eliminate unphysical edge effects.

2. FFTBM improvement by signal mirroring

FFTBM performs comparison between the calculated and experimental time trends in frequency domain for selected TH variables. The FFTBM makes it possible to obtain a numerical judgment about the accuracy of individual TH variables as well as the overall results of the calculation (Petruzzi and D'Auria, 2008). FFTBM provides normalized and non-dimensional results, which are independent from the transient duration (Del Nevo et al., 2012). In the following sub-sections, after an introduction to original FFTBM, FFTBM-SM and its role in improvement of the accuracy assessment are briefly described. For further explanations, readers are referred to D'Auria et al. (1994), Prošek et al. (2002), and Prošek et al. (2008).

2.1. Description of original FFTBM

Quantification of the accuracy for an individual variable, is based on amplitudes of discrete experimental and error signals provided by fast Fourier transform at frequencies f_n, where n = (0,1,2,...2^m) and m is the exponent specifying the number of points ($N = 2^{m+1}$) (Prošek et al., 2006). The error function is defined as $\Delta F(t) = F_{calc}(t) - F_{exp}(t)$ in the time domain where $F_{exp}(t)$ and $F_{calc}(t)$ are experimental and calculated signals, respectively. Dimensionless Average Amplitude (AA) is considered as average fractional error of the calculation where $\Delta\tilde{F}(f_n)$ is the error function amplitude at frequency f_n, and $\tilde{F}_{exp}(f_n)$ is the time function amplitude at frequency f_n:

$$AA = \frac{\sum_{n=0}^{2^m} |\Delta\tilde{F}(f_n)|}{\sum_{n=0}^{2^m} |\tilde{F}_{exp}(f_n)|} \quad (1)$$

Dimensionless Weighted Frequency (WF) gives an idea of the frequencies related to the inaccuracy (Shahedi et al., 2010):

$$WF = \frac{\sum_{n=0}^{2^m} |\Delta\tilde{F}(f_n)| \cdot f_n}{\sum_{n=0}^{2^m} |\Delta\tilde{F}(f_n)|} \quad (2)$$

For a variable, better accuracy is represented by low AA values at high WF values (Prošek et al., 2004). The overall judgment of the calculation accuracy is obtained by defining average performance indices, i.e. total weighted average amplitude (AA_{tot}) and total weighted frequency (WF_{tot}):

$$AA_{tot} = \sum_{i=1}^{N_{var}} (AA)_i (W_f)_i \quad (3)$$

$$WF_{tot} = \sum_{i=1}^{N_{var}} (WF)_i (W_f)_i \quad (4)$$

with

$$(W_f)_i = \frac{(W_{exp})_i \times (W_{saf})_i \times (W_{norm})_i}{\sum_{j=1}^{N_{var}} (W_{exp})_j \times (W_{saf})_j \times (W_{norm})_j} \quad \text{and} \quad \sum_{i=1}^{N_{var}} (W_f)_i = 1 \quad (5)$$

where N_{var} is the number of the variables analyzed. $(WF)_i$, $(AA)_i$, $(W_f)_i$ are weighted frequency, average amplitude, and weighting factor for ith analyzed variable, respectively. Each weighting factor (W_f) accounts for safety relevance of a particular variable (W_{saf}), experimental accuracy (W_{exp}) and the variable relevance to primary pressure (W_{norm}). Selected weighting factor components for typical TH variables are given in Table 1 (Shahedi et al., 2010).

For the total accuracy, the following criteria were defined (Prošek et al., 2002):

- $AA_{tot} \leqslant 0.3$: characterize very good code predictions,
- $0.3 < AA_{tot} \leqslant 0.5$: characterize good code predictions,
- $0.5 < AA_{tot} \leqslant 0.7$: characterize poor code predictions, and
- $AA_{tot} > 0.7$: characterize very poor code predictions.

Because of difficulties in reaching $AA_{tot} \leqslant 0.3$ (e.g. very good knowledge of boundary conditions and a very detailed nodalization), $AA_{tot} = 0.4$ was selected as an acceptability limit of calculations for the whole transient (Prošek et al., 2002).

2.2. Accuracy assessment in a series of time-intervals

In original FFTBM, accuracy assessment is usually carried out for a limited number of time-intervals where each one is based a phenomenological window. The time-intervals start at the beginning of transients and end at expiration time of each phenomenological window (Prošek et al., 2002). Prošek et al. (2006) proposed a methodology for using a series of time-intervals instead of a few phenomena-based time windows. This provides deeper insights into how accuracy changes during the transient. There are two methods for defining the time-intervals: (1) moving time window: whole transient duration is divided into a set of narrow time-intervals with same length, and (2) increasing time window: a set of time-intervals are defined, each expanded for duration of one narrow time-interval related to the previous window, thus last one covers the whole transient duration (Prošek et al., 2006). The first approach presents instantaneous discrepancies between experimental data and calculated results, while the second indicates integral accuracy variation as a function of accident progression time.

Table 1
Selected weighting factor components for typical TH variables.

Variable	W_{exp}	W_{saf}	W_{norm}
Primary pressure	1.0	1.0	1.0
Secondary pressure	1.0	0.6	1.1
Pressure drops	0.7	0.7	0.5
Mass inventories	0.8	0.9	0.9
Flow rates	0.5	0.8	0.5
Fluid temperatures	0.8	0.8	2.4
Clad temperatures	0.9	1.0	1.2
Collapsed levels	0.8	0.9	0.6
Core power	0.8	0.8	0.5

2.3. FFTBM-SM

In implementation of original FFTBM, it is revealed that there is an unphysical edge effect on FFTBM results when experimental signals sharply increase or decrease (Prošek et al., 2008). Fluctuations in the accuracy index (AA) of original FFTBM caused by the difference (edge) between the first and last data points of the investigated signals (Prošek and Leskovar, 2015). Discrete Fourier transform used in the FFTBM, considers the time-dependent signal as an infinite periodic signal (Fig. 1). The frequencies coming from such artificial edge in infinite periodic signals of the error function ($\Delta F(t) = F_{calc}(t) - F_{exp}(t)$) or experimental signal ($F_{exp}(t)$) may considerably affect the accuracy index in Eq. (1). Signal mirroring enables to have symmetrized signals with the identical characteristics without introducing the edge, when treated as an infinite periodic signal (Fig. 1) (Prošek and Leskovar, 2015). Thus, FFTBM-SM can eliminate the fluctuations in accuracy assessment of TH codes, especially when performing assessments for a large number of time-intervals.

To investigate the effect of signal mirroring on the numerator and denominator of the total accuracy index in Eq. (1), two definitions are proposed by Prošek et al. (2008) for average amplitude of error function (AA_{err}) and experimental signal (AA_{exp}):

$$AA_{err} = \frac{1}{2^m + 1} \sum_{n=0}^{2^m} |\Delta \tilde{F}(f_n)| \quad (6)$$

$$AA_{exp} = \frac{1}{2^m + 1} \sum_{n=0}^{2^m} |\tilde{F}_{exp}(f_n)| \quad (7)$$

These definitions are used in Section 3.2 to analyze the differences between accuracy indices calculated by the original FFTBM and FFTBM-SM.

3. Accuracy assessment of MELCOR code using FFTBM-SM

In this section, after an introduction to PSB-VVER ITF and its TH nodalization for modeling SBO accident by MELCOR code, the results of accuracy evaluation by original FFTBM and FFTBM-SM are presented, when phenomena-based time intervals are used. Then, the results of accuracy assessment by FFTBM-SM in a series of time-intervals are presented, and compared with those of original FFTBM.

3.1. Nodalization and modeling of PSB-VVER ITF by MELCOR code

PSB-VVER is a large-scale ITF which simulates Russian-designed light water reactor NPPs, VVER-1000, on a scale of 1:300 in terms of the core thermal power and overall volume of primary system with the same height elevations (Kroshilin et al., 2006). PSB-VVER ITF models the entire primary system and most of the secondary system (Fig. 2) including: the reactor pressure vessel, four separate circulation loops, the pressurizer, the Steam Generators (SGs) and the Main Coolant Pumps (MCPs) (Bucalossi et al., 2012). Also, safety systems such as emergency feed water system, emergency core cooling systems, safety/relief valves of the pressurizer, automatic depressurization valves (BRU-A), SG isolation valves and the turbine stop valve are available in PSB-VVER ITF.

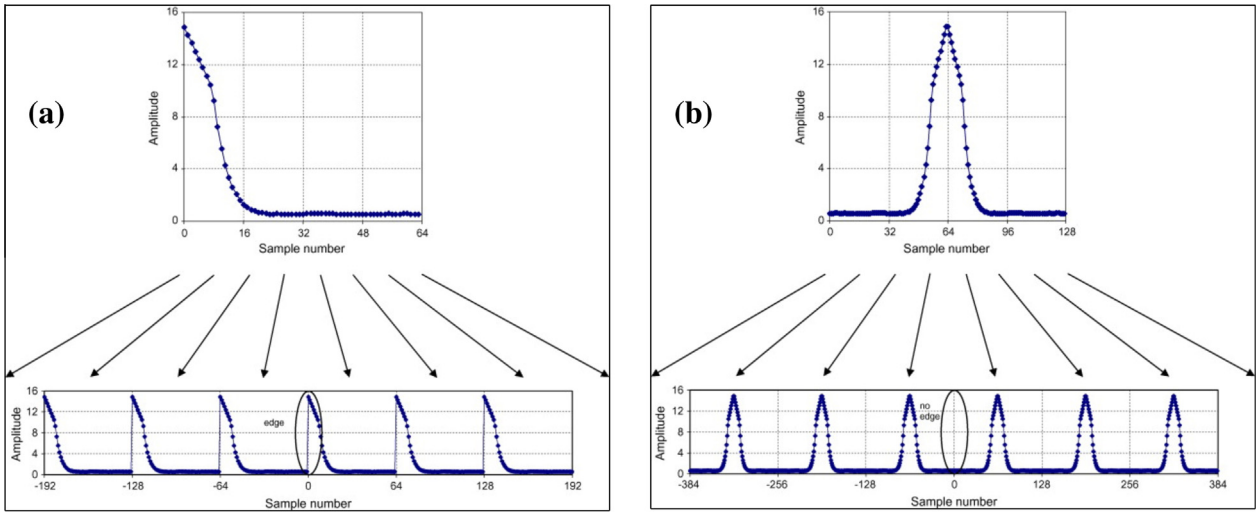

Fig. 1. Comparison between (a) original signal and (b) symmetrized signal by signal mirroring: Upper figures show the time domain with N samples length and lower figures show infinite periodic signals (Prošek et al., 2008).

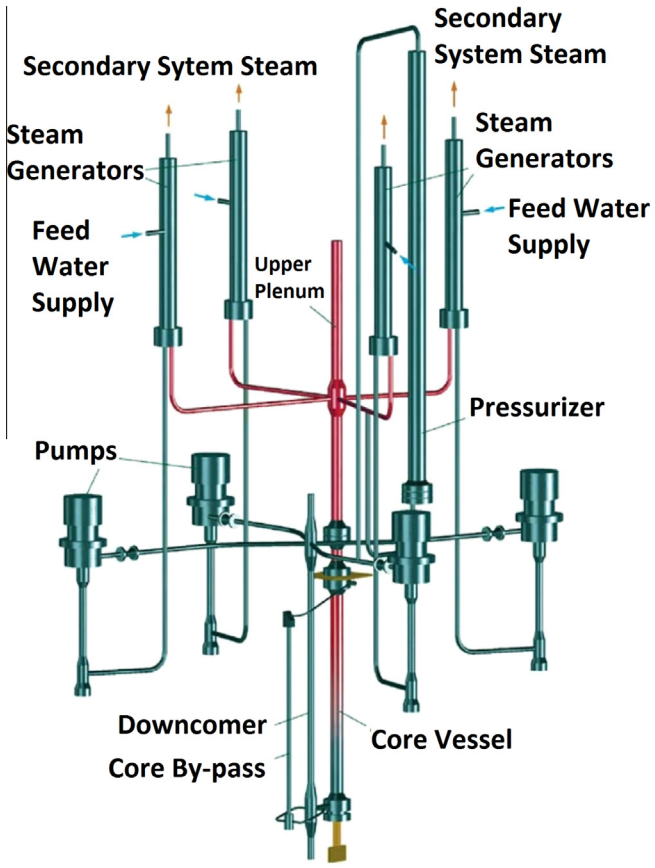

Fig. 2. PSB-VVER integral test facility.

Nodalization is the result of a challenging process which requires a suitable understanding of the NPP and of the code nature and structure (D'Auria and Galassi, 2010). The majority of existing TH system codes follow the concept of a "free nodalization," which means, the code users have to build up a detailed noding diagram which maps the whole system to be calculated into the frame of a one-dimensional TH network (Petruzzi and D'Auria, 2008). A TH nodalization for modeling PSB-VVER ITF by MELCOR code (Fig. 3) was previously developed and qualified at both steady-state and transient levels (Saghafi et al., 2016). The accuracy of the MELCOR predictions with the developed nodalization were qualitatively and quantitatively evaluated. The developed nodalization reproduced the relevant thermal-hydraulic aspects at the transient level and had acceptable accuracy index calculated with original FFTBM.

The test performed is a SBO with operator actions on secondary side cooling of SGs, i.e. depressurizing and water injection. During this test, various TH phenomena were observed, including: heat transfer in the covered core, natural circulation of single and two phase flow, asymmetrical loops behavior, heat transfer between primary and secondary sides of SGs, etc. Generally, the test is subdivided into 5 phenomenological windows (D'Auria et al., 2006).

1. The events occurring at the beginning of the transient are: stop of the steam dumping from SGs, isolation of the feed water valves, core power switching off simulating scram, MCPs start to coast-down, and PRZ heater power is changed for the heat losses compensation. Soon after the beginning of the test, pressure of the SGs starts to increase, and the first opening of BRU-A valves occurs.
2. Decreasing level of all SGs reduces the heat transfer rate from primary to secondary and increases temperature and pressure of the primary circuit. This leads to an increase in water volume of the primary circuit and in water level of the PRZ.
3. The set point for opening of the Power Operated Relief Valve (PORV) of PRZ is reached and it starts to cycle. Steam dump from the PORV is not sufficient to cool-down the primary system, after that the SGs are completely empty. Therefore, the coolant temperature continues to increase and leads to cladding temperature increase. At the end of this phenomenological window, the cladding temperature reaches to 350 °C, which is the signal for accident management procedure activation.
4. The BRU-A valves of SG #1 and SG #4 are fully open and the Fast Acting Steam Isolating Valves (FASIVs) on the steam line #2 and steam line #3 are closed. The pressure in the SG #1 and SG #4 rapidly decreases, while in the other SGs, it remains constant.
5. When the pressure in the SG #1 reaches 1 MPa, the feed water starts to inject in secondary side of SG #1. Then, the PORV stops to cycle and the coolant temperature starts to decrease.

Time sequence of significant events in the MELCOR simulation is compared with SBO experimental data (Müllner, 2010) in Table 2. Also, phenomenological windows of the accident simulation are

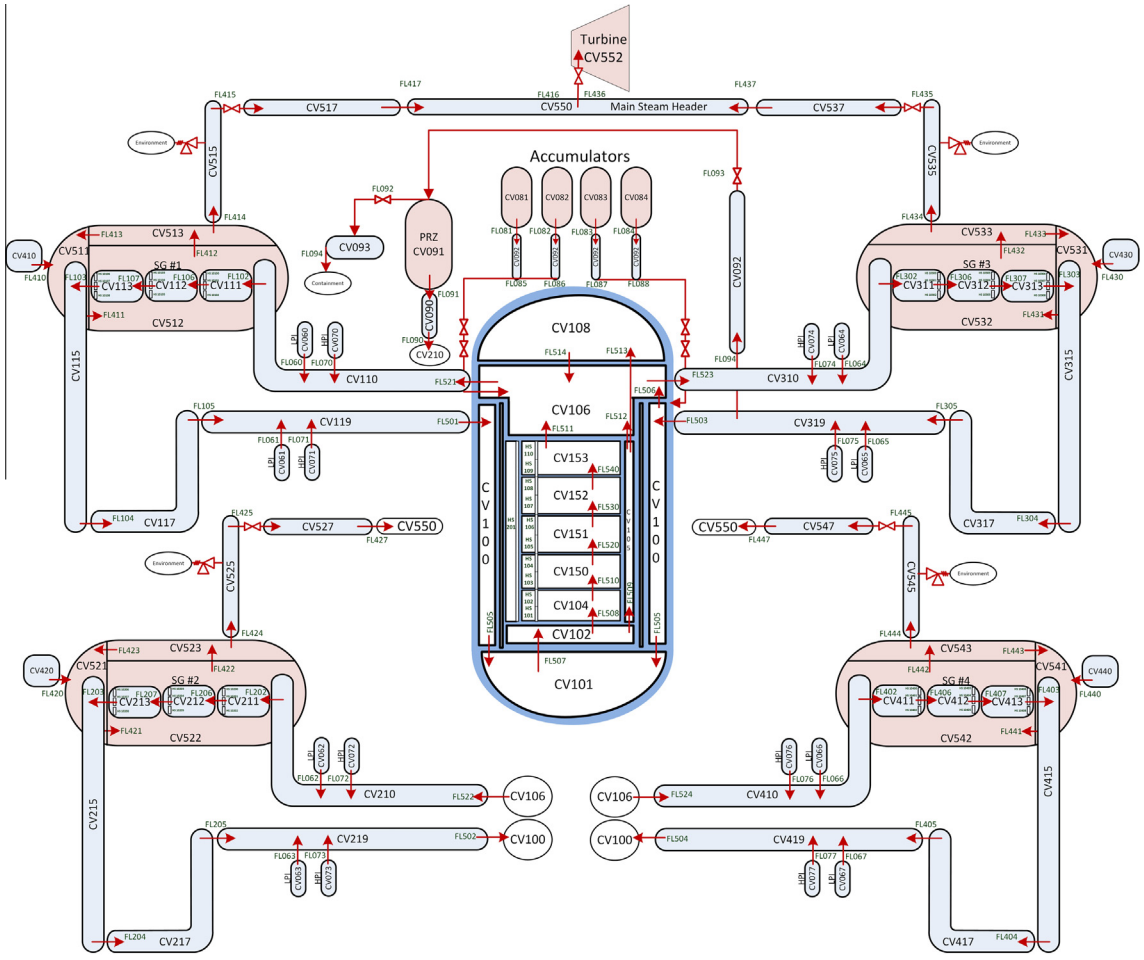

Fig. 3. Nodalization of PSB-VVER ITF.

Table 2
Time sequences of the main events.

Event	PSB-VVER ITF experiment Time (s)	MELCOR simulation Time (s)
Start of test	0	0
Stop of PRZ heater power change	0	0
Start of closing steam discharge valve	0	0
Start of MCP coast-down	0	0
Start of core and core by-pass reduction	5.6	5.6
Complete closing of feed water valve of SG #1	6	10
Complete closing of feed water valve of SG #2	11	10
Complete closing of feed water valve of SG #3	15	10
Complete closing of feed water valve of SG #4	7	10
Stopping of SG steam discharge	16	16
First ADS operation	200–219	136
Complete switching off of MCP	232	232
First PRZ relief valve operation	6315–6327	5137
Closure of FASIV in SG #2 and SG #3	10014	9943
Opening of ADS in SG #1 and SG #4	10029	9943
Water supply into SG #1	10282	9994
Stop of experiment	15016	15000

compared with PSB-VVER experiment data (D'Auria et al., 2006) in Table 3.

3.2. Results and discussion

Accuracy assessment of MELCOR code has been made with original FFTBM and FFTBM-SM, using 28 TH variables selected considering peculiarities of the transient, as well as the quality and availability of experimental data. For comparison of the results, 5 time-intervals were selected considering phenomenological windows of SBO accident in PSB-VVER ITF (Table 4). The total accuracy index (AA_{tot}) is in the acceptable range in all time-intervals, for both original FFTBM and FFTBM-SM (Fig. 4).

Table 3
Phenomenological windows of SBO accident in PSB-VVER ITF.

No	Event	PSB-VVER ITF experiment Time (s)	MELCOR calculation Time (s)
1	BRU-A opening and closure	0–232	0–232
2	Primary pressure constant	232–5146	232–3175
3	Primary pressure increases	5146–10029	3175–9943
4	Depressurization of SG #1 and SG #4	10029–10282	9943–9994
5	Injection to secondary side of SG #1	10282–15016	9994–15000

For improvement of accuracy assessment, a series of increasing time-intervals were used, in which the duration of each time-interval, starting at 0 s, is expanded by 50 s. In this way, 300 time-intervals were created to perform accuracy assessment for the whole transient. In the following, experimental data and the MELCOR results, for 28 TH variables, are compared as well as the results of accuracy assessment by original FFTBM (AA) and FFTBM-SM (AA_m):

Table 4
Accuracy evaluation of the TH variables using original FFTBM and FFTBM-SM.

No	Variable	(0 s–232 s)		(0 s–5146 s)		(0 s–10029 s)		(0 s–10282 s)		(0 s–15000 s)	
		AA	AA_m	AA	AA_m	AA	AA_m	AA	AA_m	AA	AA_m
1	Loop #1 mass flow rate	0.354	0.495	0.407	0.631	0.513	0.686	0.828	1.044	0.731	0.879
2	Loop #2 mass flow rate	0.247	0.367	0.363	0.537	0.409	0.585	0.447	0.623	0.450	0.634
3	Loop #3 mass flow rate	0.303	0.437	0.344	0.560	0.440	0.621	0.494	0.641	0.476	0.661
4	Loop #4 mass flow rate	0.245	0.379	0.313	0.491	0.387	0.561	0.623	0.735	0.609	0.851
5	Pressure in pressurizer	0.014	0.012	0.408	0.257	0.430	0.506	0.452	0.534	0.442	0.535
6	Pressure in UP	0.022	0.017	0.384	0.245	0.356	0.444	0.403	0.484	0.387	0.486
7	Clad maximum temp.	0.084	0.102	0.137	0.137	0.127	0.140	0.118	0.141	0.130	0.143
8	Coolant temp. at core inlet	0.016	0.016	0.143	0.062	0.056	0.068	0.046	0.072	0.061	0.084
9	Coolant temp. at core outlet	0.033	0.041	0.132	0.096	0.083	0.103	0.076	0.106	0.089	0.108
10	Level in PRZ	0.115	0.094	0.204	0.248	0.411	0.440	0.408	0.446	0.512	0.469
11	Level in SG #1	0.297	0.360	0.199	0.596	0.208	0.593	0.211	0.596	0.219	0.597
12	Level in SG #2	0.309	0.357	0.202	0.583	0.210	0.574	0.210	0.573	0.212	0.563
13	Level in SG #3	0.302	0.375	0.201	0.620	0.213	0.622	0.214	0.627	0.219	0.617
14	Level in SG #4	0.306	0.354	0.211	0.608	0.219	0.600	0.219	0.601	0.222	0.590
15	Pressure in SG #1	0.199	0.222	0.646	0.751	1.094	0.971	0.697	0.940	0.516	0.741
16	Pressure in SG #2	0.199	0.227	0.646	0.751	0.678	0.762	0.680	0.758	0.671	0.774
17	Pressure in SG #3	0.203	0.222	0.646	0.750	0.678	0.762	0.678	0.756	0.662	0.772
18	Pressure in SG #4	0.203	0.223	0.646	0.751	1.092	0.972	0.691	0.938	0.506	0.730
19	PD across core	0.119	0.141	0.216	0.244	0.170	0.251	0.173	0.259	0.227	0.296
20	PD across UP	0.160	0.144	0.212	0.260	0.234	0.281	0.245	0.289	0.264	0.303
21	PD in loop seal #1	0.109	0.113	0.218	0.221	0.168	0.257	0.202	0.293	0.279	0.327
22	PD in loop seal #2	0.104	0.111	0.215	0.223	0.159	0.243	0.164	0.252	0.232	0.301
23	PD in loop seal #3	0.113	0.122	0.219	0.228	0.177	0.262	0.182	0.271	0.236	0.304
24	PD in loop seal #4	0.106	0.114	0.217	0.224	0.169	0.256	0.177	0.267	0.232	0.301
25	Coolant temp. at Upper Head	0.049	0.043	0.135	0.046	0.106	0.049	0.104	0.050	0.223	0.084
26	Clad temp. at bottom level	0.059	0.062	0.140	0.125	0.125	0.138	0.115	0.138	0.130	0.142
27	Clad temp. at middle level	0.052	0.058	0.122	0.108	0.119	0.119	0.109	0.120	0.126	0.123
28	Clad temp. at 2/3 core height	0.068	0.080	0.136	0.126	0.111	0.129	0.108	0.129	0.124	0.131
	Total	0.110	0.127	0.264	0.293	0.288	0.347	0.267	0.356	0.273	0.350

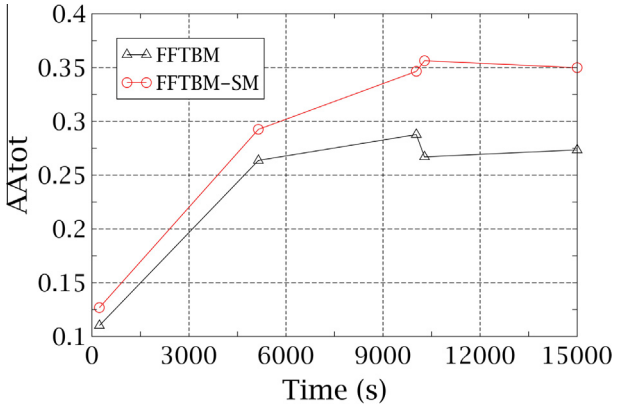

Fig. 4. Total weighted average amplitudes (AA_{tot}) for 5 time-intervals.

- Calculated coolant mass flow rate of the primary loops together with experimental data are illustrated in Fig. 5. MELCOR predictions show the same experimental time-trend until the third phenomenological window, but followed by significant discrepancies. The results of accuracy assessment, i.e. AA and AA_m, for coolant mass flow rate in the primary loops are shown in Fig. 6. Both accuracy indices increase when discrepancies appear between the MELCOR predictions and experimental data, especially in the loops with depressurized SG.
- Pressure in the PRZ and UP are presented in Fig. 7. MELCOR predicts pressure increase in the primary system and earlier operation of PORV compared to the experimental results. Fig. 8 shows the variation of AA and AA_m of primary pressures during the transient. It can be seen that, when periodic operation of PORV causes an oscillating behavior in primary pressures, AA also follows this trend, while AA_m is not affected from triangular shape of the pressure signal.

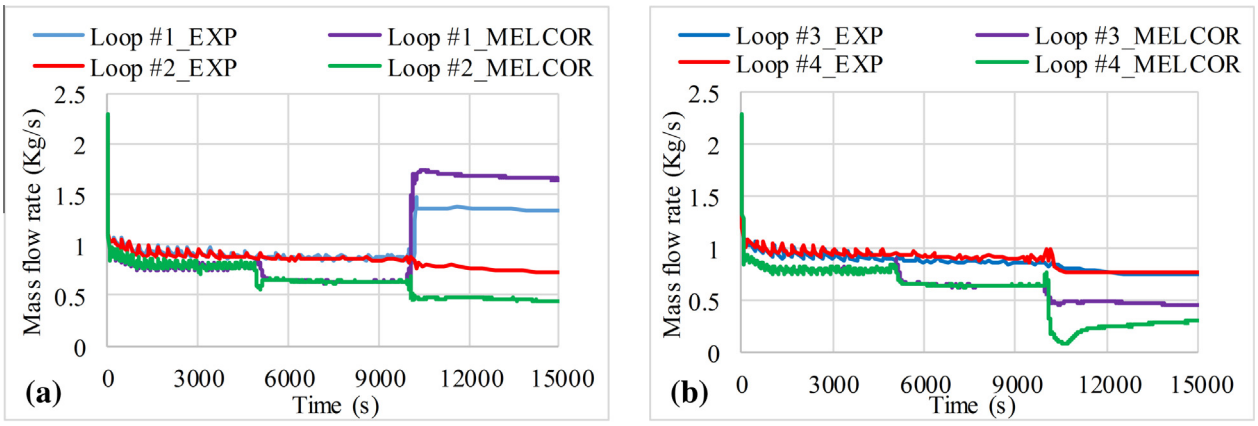

Fig. 5. Coolant mass flow rate in the primary loops: (a) Loop #1, Loop #2, (b) Loop #3 and Loop #4.

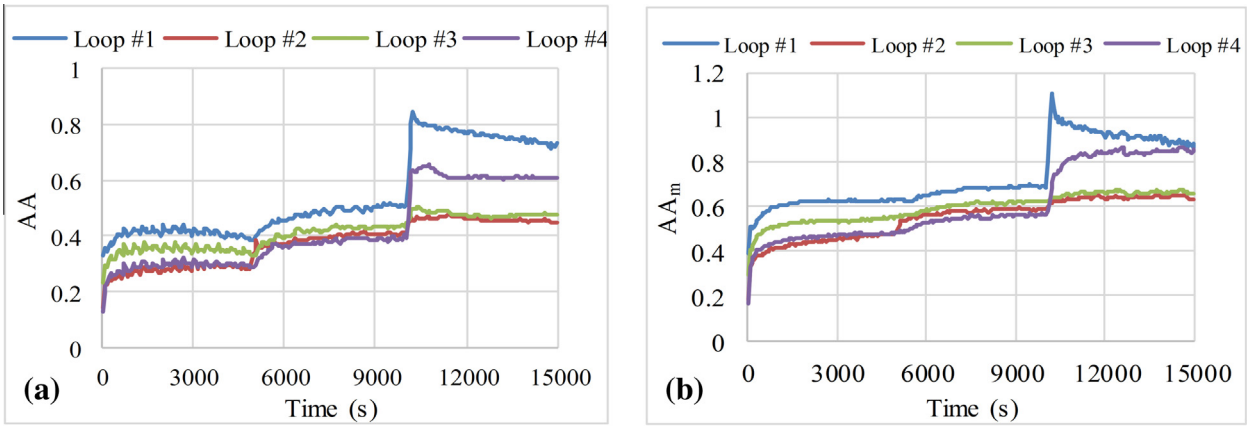

Fig. 6. AA of coolant mass flow rate in the primary loops: (a) FFTBM and (b) FFTBM-SM.

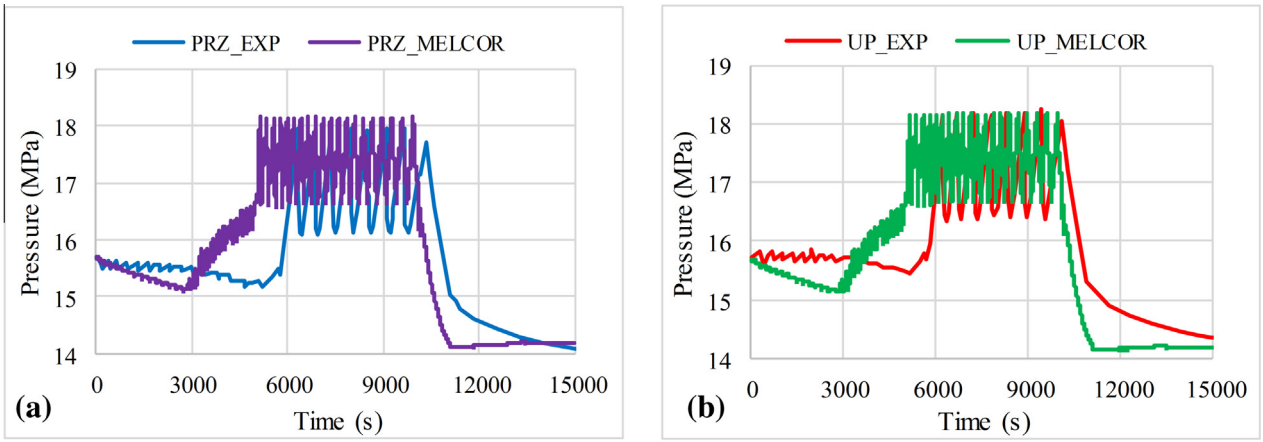

Fig. 7. Pressure of (a) the PRZ and (b) the UP.

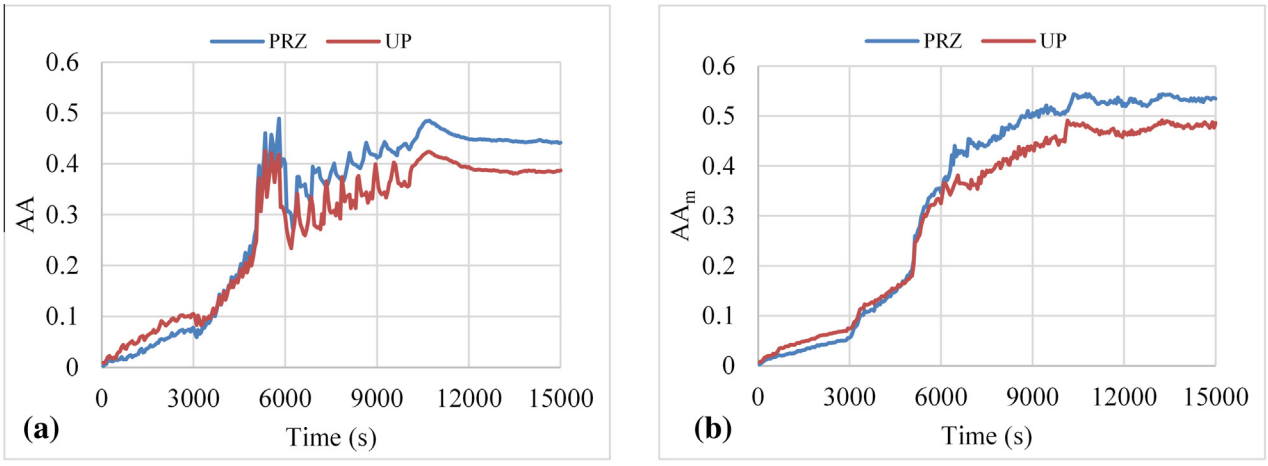

Fig. 8. AA of PRZ and UP Pressure: (a) FFTBM and (b) FFTBM-SM.

- In Figs. 9 and 11, temperature in different elevations of the core for coolant and fuel cladding are illustrated, respectively. These figures show the maximum clad and coolant temperatures are well simulated by MELCOR code. After reaching a maximum, temperatures drop because of accident management measures, i.e. depressurization and water injection to the secondary side. Small deviations of calculated coolant and clad temperatures from experimental data lead to have small values for both AA and AA_m in Figs. 10 and 12, respectively.
- Pressure drop across the core, UP and loop seals are shown in Fig. 13, and the related average amplitudes are compared in Fig. 14. These pressure drops increase until a maximum value,

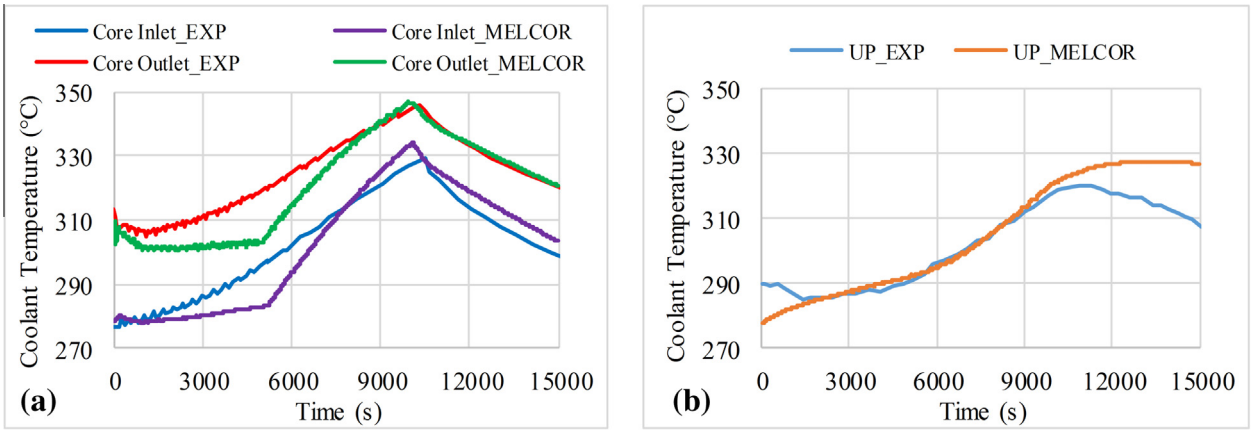

Fig. 9. Coolant temperature at (a) core inlet and outlet, and (b) UP.

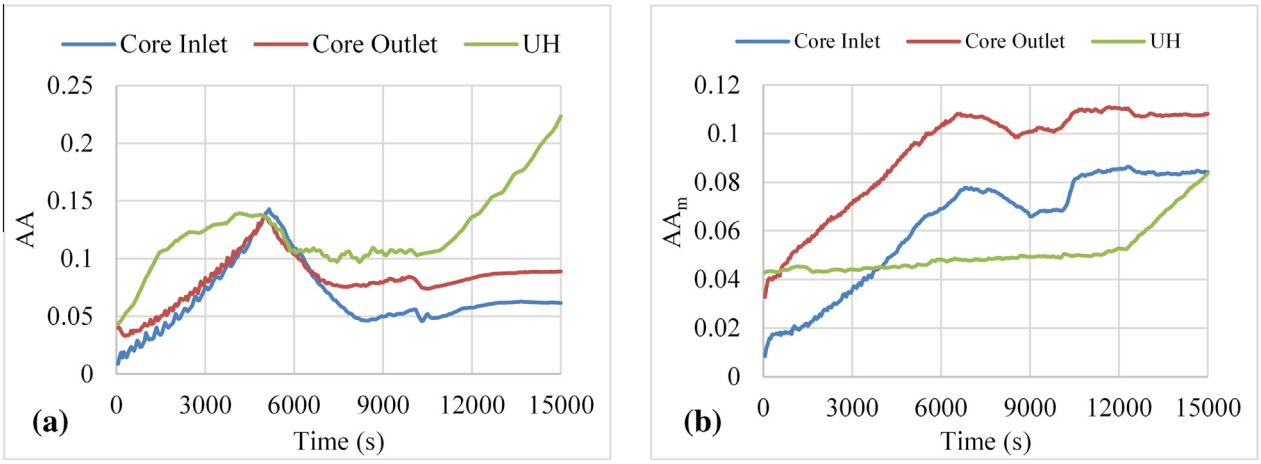

Fig. 10. AA of coolant temperature at the UP, the core inlet and outlet: (a) FFTBM and (b) FFTBM-SM.

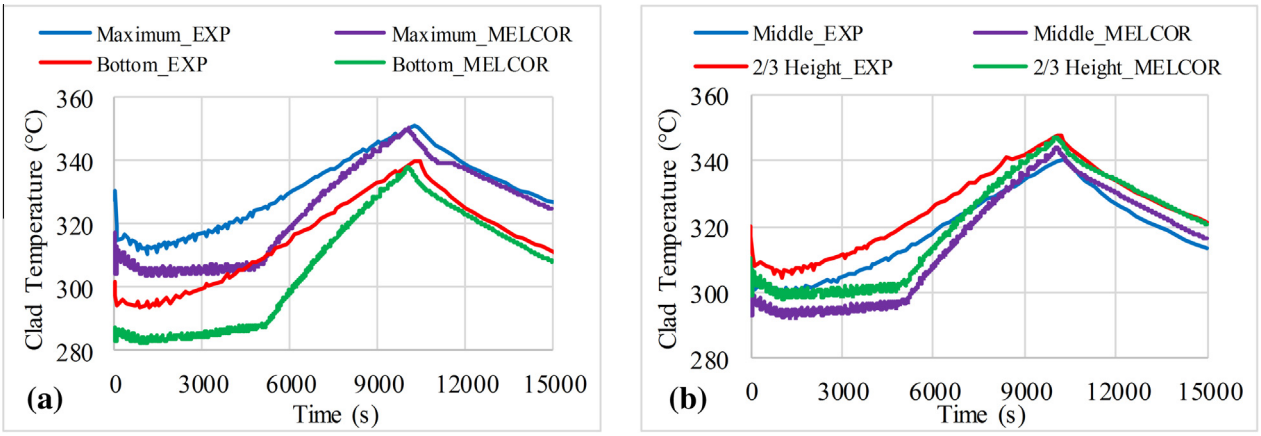

Fig. 11. Temperature of fuel cladding: (a) maximum point, bottom level, (b) middle level and 2/3 core height.

which is related to the maximum temperature and minimum density of the primary coolant. While AA increases when the difference between experimental and calculated results increased (and *vice versa*), AA_m maintains more reasonable trend, i.e. almost increasing, for the whole transient duration.

- Variation of the predicted collapsed water level of the PRZ and SGs is compared with experimental data in Fig. 15. MELCOR mostly over-predicted collapsed water level of the PRZ. The AA and AA_m for collapsed water level of the PRZ and SGs are presented as a function of time in Fig. 16. After SGs dry-out, AA and AA_m are not changed anymore, because the collapsed water level approximately remains constant.
- Pressure of secondary side of the SGs and the related average amplitudes are illustrated in Figs. 17 and 18, respectively. In SG #1 and SG #4, pressure drops to atmospheric pressure due to operator actions in the opening of BRU-A valves. Earlier

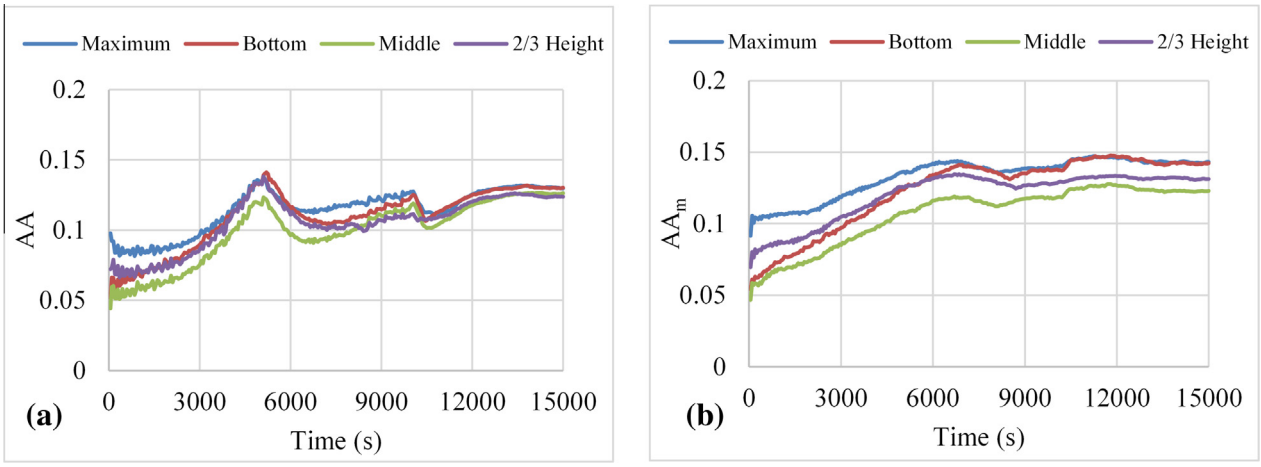

Fig. 12. AA of the clad temperature at the maximum point, bottom level, middle level and 2/3 core height: (a) FFTBM and (b) FFTBM-SM.

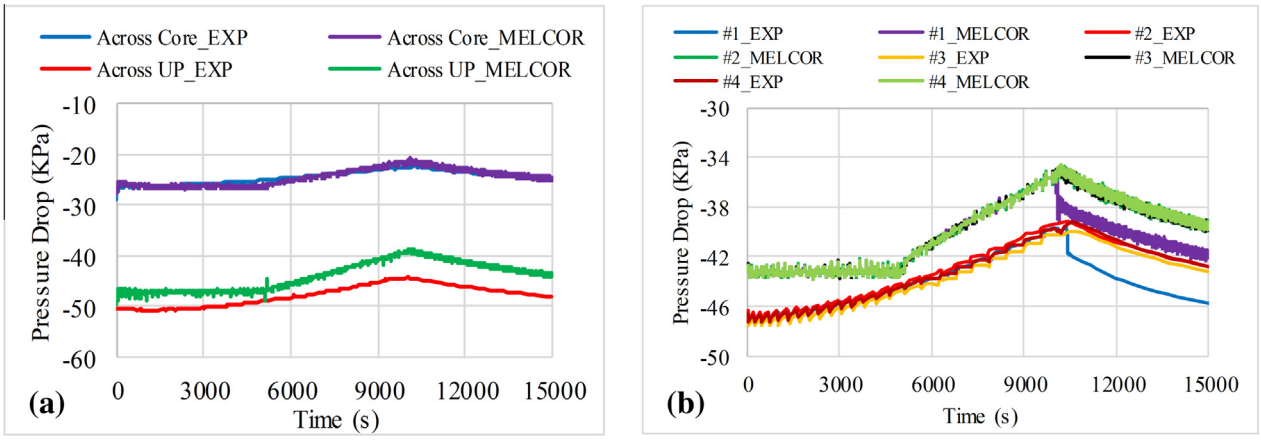

Fig. 13. Pressure drop across (a) the core, the UP, (b) Loop seal #1, Loop seal #2, Loop seal #3 and Loop seal #4.

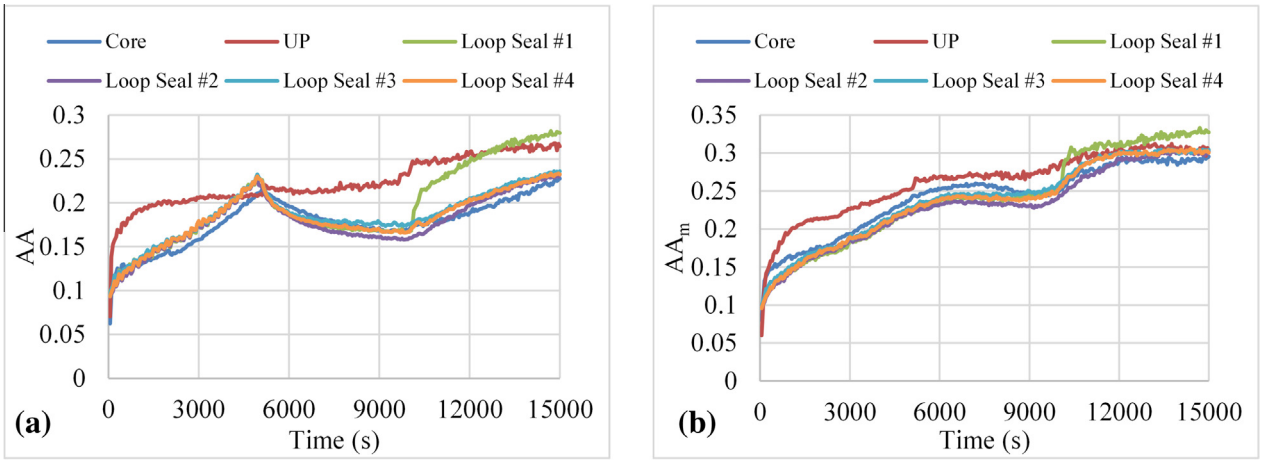

Fig. 14. AA of pressure drop across the core, the UP, Loop seals: (a) FFTBM and (b) FFTBM-SM.

depressurization in the MELCOR simulation, leads to considerable decrease of accuracy in a short time-interval.

The above results indicate that the accuracy index of original FFTBM, is more affected by small fluctuations of the TH variables than FFTBM-SM.

In Table 5, average amplitudes of the error function and experimental signal are presented for the all TH variables considered for original FFTBM, AA_{err} and AA_{exp}, and FFTBM-SM, AA_{err_m} and AA_{exp_m}. Influence of unphysical edge elimination by FFTBM-SM from the error function and experimental signal are expressed by AA_{err}/AA_{err_m} and AA_{exp}/AA_{exp_m}, respectively. These ratios vary

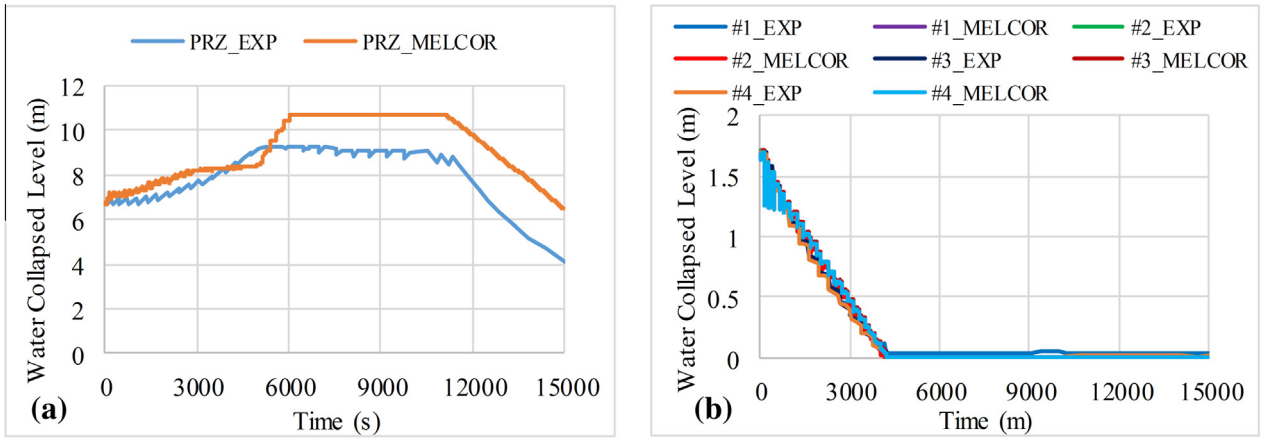

Fig. 15. Collapsed water level of (a) the PRZ, (b) SG #1, SG #2, SG #3 and SG #4.

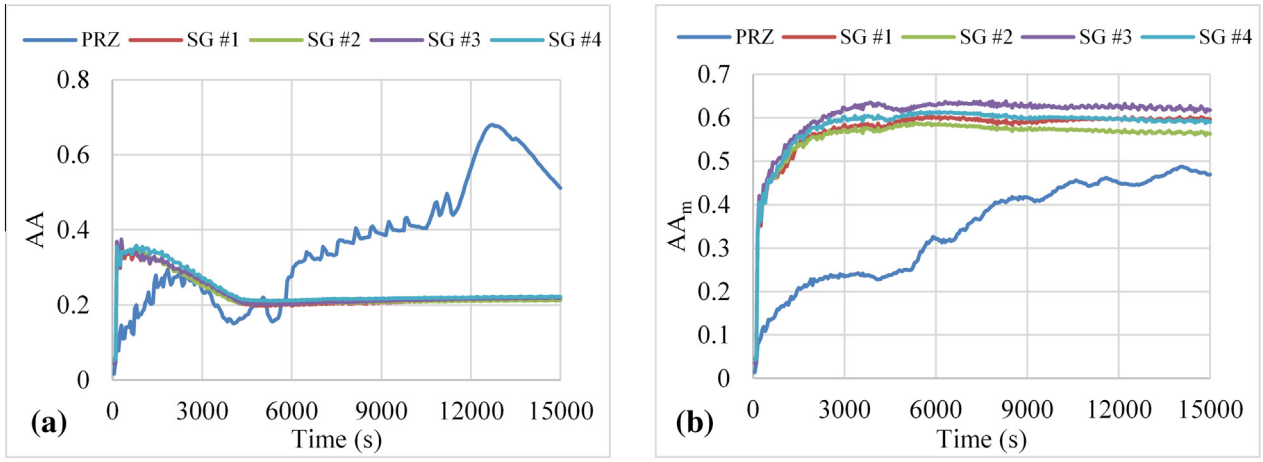

Fig. 16. AA of collapsed water level in the PRZ and SGs: (a) FFTBM and (b) FFTBM-SM.

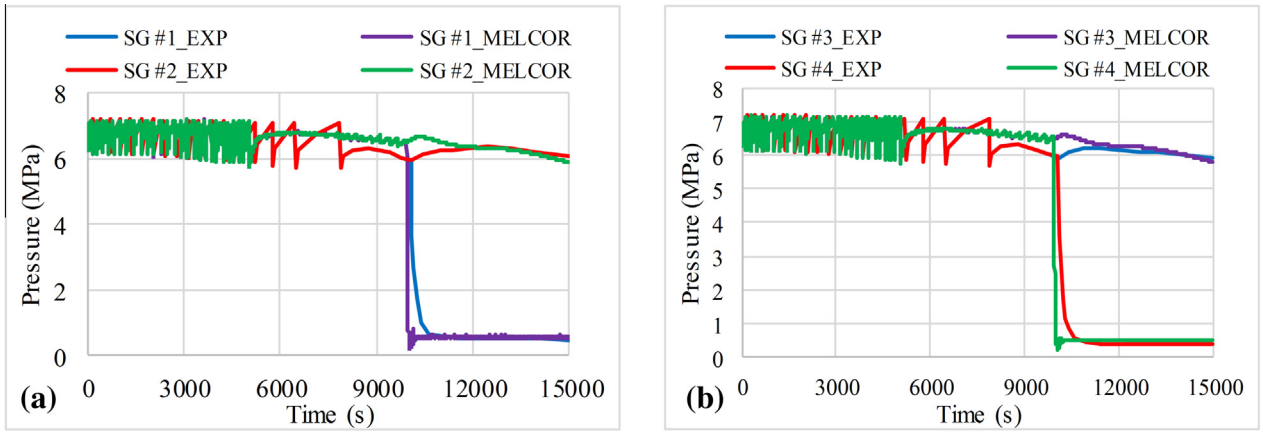

Fig. 17. Pressure of (a) SG #1, SG #2, (b) SG #3 and SG #4.

between 1.530 and 5.804, because of different edge effects on the error function and experimental signal of different TH variables. AA_{err}/AA_{err_m} in Table 5 shows that the edge effect on error function is more dominant in the coolant temperature at the upper head and has 82.8% contribution in accuracy index calculated by original FFTBM (AA_{err}). Also, AA_{exp}/AA_{exp_m} indicates that most dominant edge effect on experimental signal is related to the water level of the SGs. Experimental signal of SGs water level has approximately 77% edge contribution in the accuracy index of original FFTBM (AA_{exp}).

In Table 6, AA and AA_m of the TH variables for whole transient duration are presented. AA_{norm} and AA_{norm_m} are calculated by normalizing AA and AA_m to their average value of all selected TH variables, respectively.

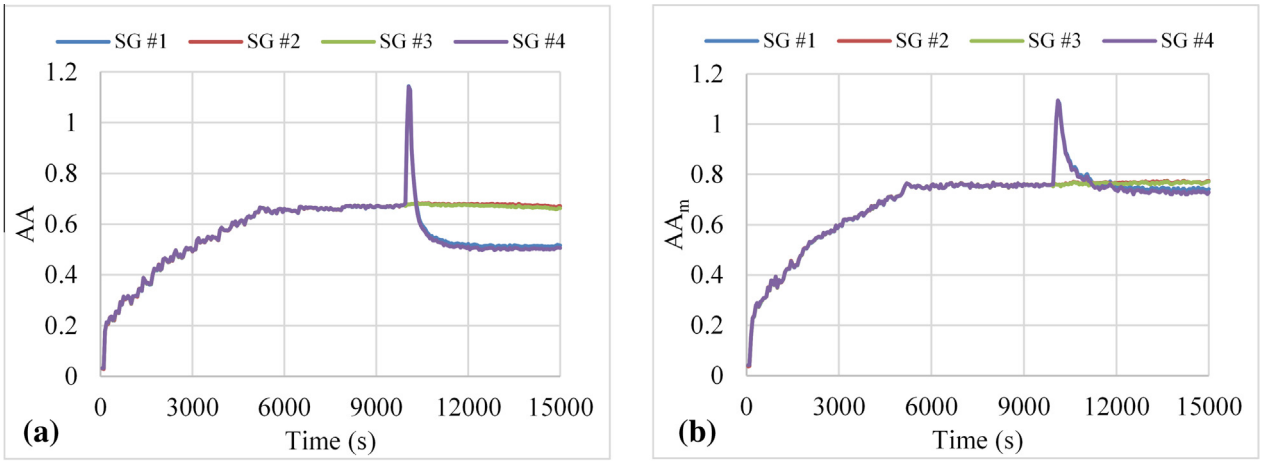

Fig. 18. AA of SGs pressure: (a) FFTBM and (b) FFTBM-SM.

Table 5
Calculation of the accuracy indices of error function and experimental signal using original FFTBM and FFTBM-SM in time interval (0–15000).

No	Variable	AA_{err}	AA_{err_m}	$\frac{AA_{err}}{AA_{err\_m}}$	AA_{exp}	AA_{exp_m}	$\frac{AA_{exp}}{AA_{exp\_m}}$
1	Loop #1 mass flow rate	0.00113	0.00071	1.606	0.00155	0.00080	1.931
2	Loop #2 mass flow rate	0.00070	0.00037	1.912	0.00155	0.00058	2.693
3	Loop #3 mass flow rate	0.00073	0.00038	1.901	0.00152	0.00058	2.638
4	Loop #4 mass flow rate	0.00098	0.00050	1.986	0.00162	0.00058	2.778
5	Pressure in pressurizer	0.00537	0.00348	1.541	0.01214	0.00651	1.864
6	Pressure in UP	0.00443	0.00289	1.530	0.01144	0.00596	1.921
7	Clad maximum temp.	0.02328	0.01328	1.754	0.17928	0.09276	1.933
8	Coolant temp. at core inlet	0.01131	0.00723	1.564	0.18395	0.08580	2.144
9	Coolant temp. at core outlet	0.01590	0.00969	1.642	0.17878	0.08960	1.995
10	Level in PRZ	0.00410	0.00151	2.719	0.00801	0.00321	2.495
11	Level in SG #1	0.00050	0.00032	1.569	0.00227	0.00053	4.280
12	Level in SG #2	0.00049	0.00030	1.595	0.00229	0.00054	4.226
13	Level in SG #3	0.00050	0.00032	1.585	0.00230	0.00052	4.460
14	Level in SG #4	0.00050	0.00032	1.587	0.00228	0.00054	4.224
15	Pressure in SG #1	0.00618	0.00392	1.576	0.01196	0.00529	2.263
16	Pressure in SG #2	0.00412	0.00263	1.568	0.00614	0.00340	1.809
17	Pressure in SG #3	0.00410	0.00262	1.568	0.00620	0.00339	1.827
18	Pressure in SG #4	0.00614	0.00389	1.579	0.01214	0.00533	2.275
19	PD across core	0.00359	0.00222	1.618	0.01576	0.00750	2.102
20	PD across UP	0.00725	0.00404	1.796	0.02742	0.01333	2.057
21	PD in loop seal #1	0.00713	0.00434	1.641	0.02550	0.01327	1.922
22	PD in loop seal #2	0.00632	0.00380	1.663	0.02720	0.01261	2.157
23	PD in loop seal #3	0.00649	0.00386	1.683	0.02752	0.01268	2.171
24	PD in loop seal #4	0.00640	0.00381	1.681	0.02756	0.01268	2.174
25	Coolant temp. at Upper Head	0.03956	0.00682	5.804	0.17713	0.08151	2.173
26	Clad temp. at bottom level	0.02335	0.01261	1.851	0.17946	0.08862	2.025
27	Clad temp. at middle level	0.02189	0.01087	2.014	0.17333	0.08840	1.961
28	Clad temp. at 2/3 core height	0.02183	0.01188	1.838	0.17619	0.09056	1.945

AA_{norm_m}/AA_{norm} in Table 6 can be considered as a correction factor, which indicates how much the accuracy indices obtained by original FFTBM need to be corrected because of the edge effect contribution (Prošek et al., 2008). These correction factors vary from 0.485 to 3.646, which are related to water level in SG #3 and coolant temperature in the upper head, respectively. When AA_{norm_m}/AA_{norm} is greater than 1, edge effect leads to too good judgment of the TH variable by original FFTBM. Also, original FFTBM gives too bad judgment, when AA_{norm_m}/AA_{norm} of the TH variable is smaller than 1. For example, coolant temperature in upper head, which shows monotonic behavior in MELCOR calculations, is judged significantly too good due to the edge effect on the error function. On the other hand, water level of SGs are judged too bad by original FFTBM because of the edge effect on the experimental signal.

In Fig. 19, accuracy indices of all TH variables calculated by both original FFTBM and FFTBM-SM for the whole transient, are compared. TH variables with oscillating behavior (e.g. water level and pressure of SGs) have larger AAs with FFTBM-SM, while other variables (e.g. temperature and pressure drop) have close values with both methods. In Fig. 20, AA of all TH variables versus their WF calculated by both original FFTBM and FFTBM-SM are illustrated for the whole transient. The numbers next to each data point in Fig. 20 are the numbers of the TH variables in Table 4 (first column). High accuracy is represented by small AAs at large WFs.

Finally, Fig. 21 presents variation of total accuracy indices, AA_{tot} (original FFTBM) and AA_{tot_m} (FFTBM-SM), in which both indices are below the acceptability criterion (0.4) during the whole transient. We observe that although both methods fulfills the accept-

Table 6
Calculation of correction factors for accuracy judgments with original FFTBM for PSB-VVER ITF in time interval (0–15000).

No	Variable	AA	AA_{norm}	AA_m	AA_{norm_m}	$\frac{AA_{norm\_m}}{AA_{norm}}$
1	Loop #1 mass flow rate	0.731	2.228	0.879	1.963	1.135
2	Loop #2 mass flow rate	0.450	1.372	0.634	1.415	0.969
3	Loop #3 mass flow rate	0.476	1.451	0.661	1.474	0.984
4	Loop #4 mass flow rate	0.609	1.855	0.851	1.900	0.976
5	Pressure in pressurizer	0.442	1.346	0.535	1.194	1.128
6	Pressure in UP	0.387	1.179	0.486	1.084	1.087
7	Clad maximum temp.	0.130	0.396	0.143	0.319	1.238
8	Coolant temp. at core inlet	0.061	0.187	0.084	0.188	0.996
9	Coolant temp. at core outlet	0.089	0.271	0.108	0.241	1.123
10	Level in PRZ	0.512	1.559	0.469	1.047	1.488
11	Level in SG #1	0.219	0.666	0.597	1.331	0.500
12	Level in SG #2	0.212	0.647	0.563	1.257	0.515
13	Level in SG #3	0.219	0.668	0.617	1.378	0.485
14	Level in SG #4	0.222	0.676	0.590	1.318	0.513
15	Pressure in SG #1	0.516	1.573	0.741	1.655	0.951
16	Pressure in SG #2	0.671	2.043	0.774	1.728	1.183
17	Pressure in SG #3	0.662	2.017	0.772	1.722	1.171
18	Pressure in SG #4	0.506	1.542	0.730	1.628	0.947
19	PD across core	0.227	0.693	0.296	0.659	1.051
20	PD across UP	0.264	0.805	0.303	0.676	1.192
21	PD in loop seal #1	0.279	0.851	0.327	0.731	1.165
22	PD in loop seal #2	0.232	0.707	0.301	0.672	1.052
23	PD in loop seal #3	0.236	0.719	0.304	0.679	1.058
24	PD in loop seal #4	0.232	0.708	0.301	0.671	1.055
25	Coolant temp. at Upper Head	0.223	0.680	0.084	0.187	3.646
26	Clad temp. at bottom level	0.130	0.396	0.142	0.318	1.248
27	Clad temp. at middle level	0.126	0.385	0.123	0.274	1.402
28	Clad temp. at 2/3 core height	0.124	0.377	0.131	0.293	1.289

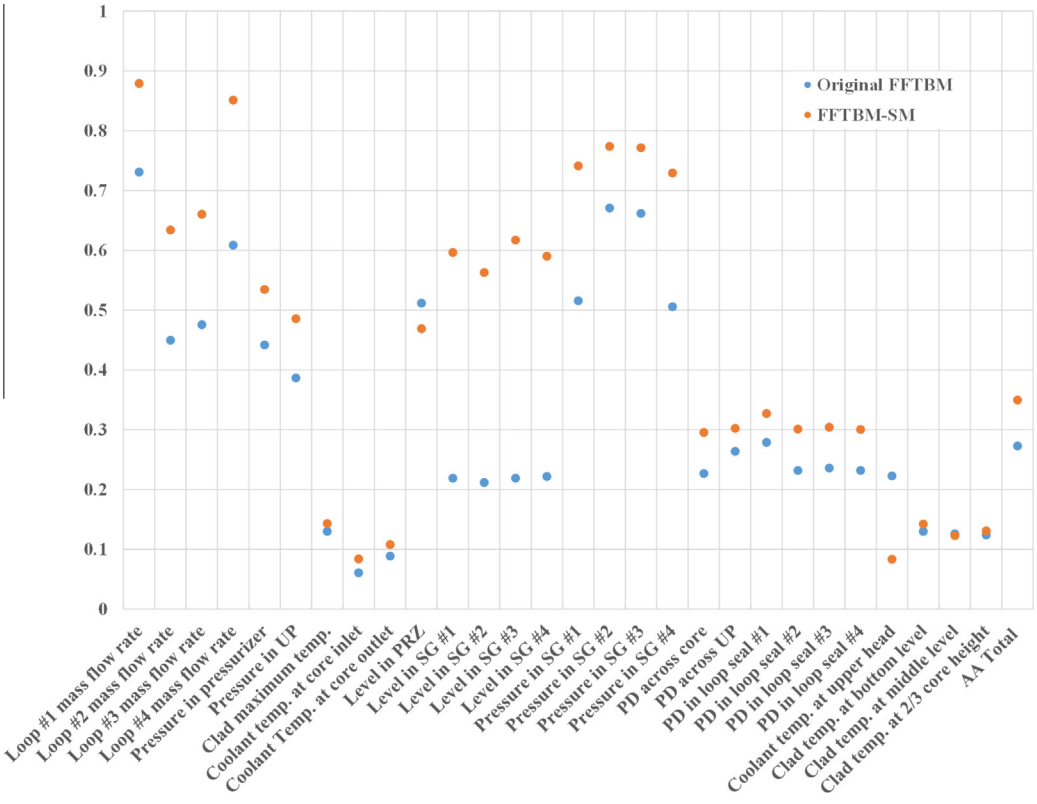

Fig. 19. Weighted average amplitudes (AA) for the whole transient.

ability criterion, original FFTBM provides smaller AA_{tot} than FFTBM-SM. In the other words, if the criteria of original FFTBM is used for FFTBM-SM, same code predictions give different levels of accuracy, i.e. "good" for FFTBMSM and "very good" for original FFTBM. Hence, considering the performance of FFTBM-SM, the criteria of the total accuracy index (AA_{tot}) for original FFTBM are not

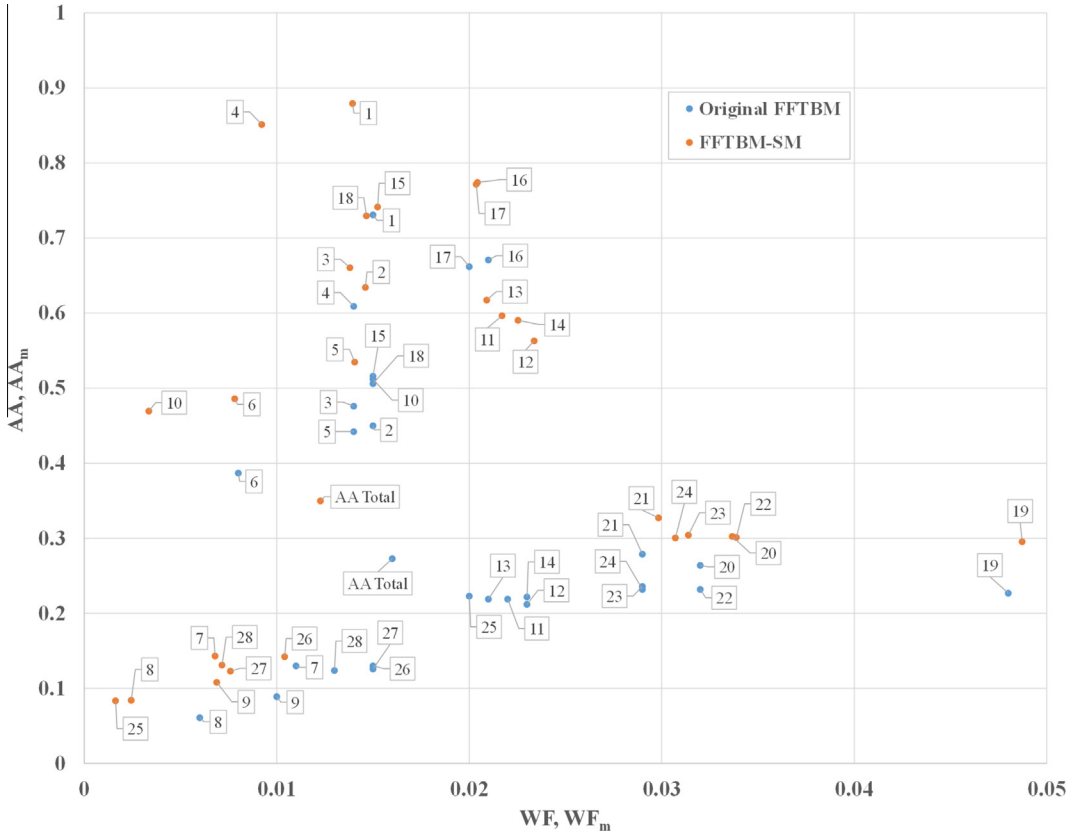

Fig. 20. Weighted average amplitudes (AA) versus weighting frequencies (WF) for the whole transient.

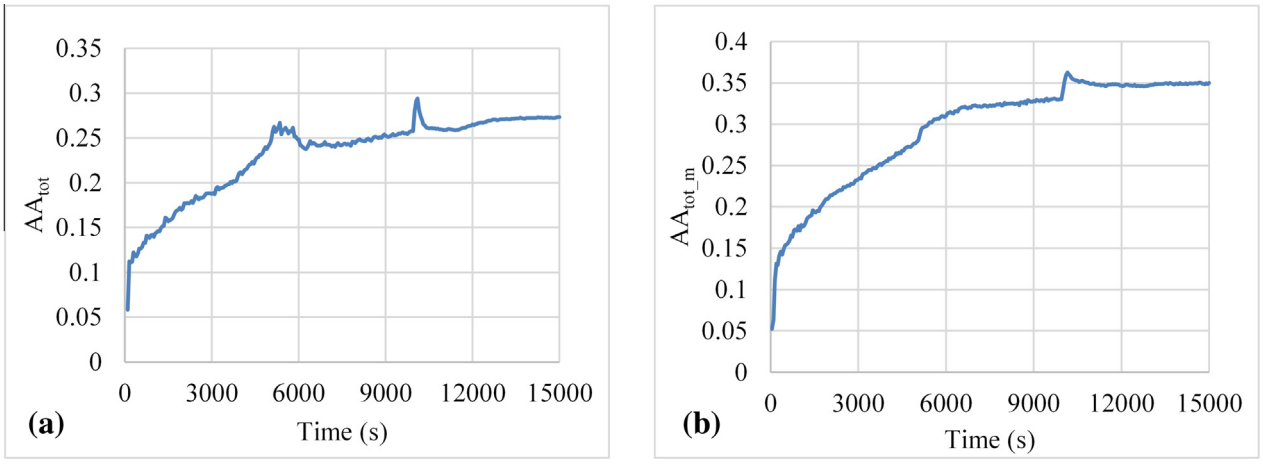

Fig. 21. Total weighted average amplitudes (AA_{tot}): (a) FFTBM and (b) FFTBM-SM.

directly applicable for FFTBM-SM and there is a need to be revised when FFTBM-SM is used.

4. Conclusion

In this paper, FFTBM-SM was applied to assess accuracy of MELCOR code for modeling SBO accident in PSB-VVER ITF. Using a series of increasing time-intervals instead of a few phenomena-based ones, provided valuable information about accuracy trend of the MELCOR predictions. When using original FFTBM, the accuracy indices fluctuate as the experimental signals sharply increase or decrease. These fluctuations were eliminated using symmetrized signals in FFTBM-SM. The results indicated the capability of FFTBM-SM to determine accuracy of the MELCOR predictions in a more realistic and consistent way than original FFTBM. However, the criteria of the total accuracy index (AA_{tot}) for original FFTBM are not directly applicable for FFTBM-SM and there is a need to be revised when FFTBM-SM is used. Nevertheless, MELCOR predictions reasonably agree with experimental data of SBO accident in PSB-VVER ITF. Hence, application of FFTBM-SM confirms that the previous TH nodalization for modeling PSB-VVER ITF by MELCOR code could be recommended for modeling SBO accident in VVER 1000 NPPs, in particular for Bushehr NPP.

References

Bucalossi, A., Del Nevo, A., Moretti, F., D'Auria, F., Elkin, I.V., Melikhov, O.I., 2012. Investigation of accident management procedures related to loss of feedwater and station blackout in PSB-VVER integral test facility. Nucl. Eng. Des. 250, 633–645.

D'Auria, F., Cherubini, M., Galassi, G., Muellner, N., 2004. Addressing the Scaling Issue by Thermalhydraulic System Codes: Recent Results, Fifth International Conference of Yugoslav Nuclear Society.

D'Auria, F., Galassi, G.M., 2010. Scaling in nuclear reactor system thermal-hydraulics. Nucl. Eng. Des. 240, 3267–3293.

D'Auria, F., Leonardi, M., Pochard, R., 1994. Methodology for the evaluation of thermalhydraulic codes accuracy. Proc. Int. Conf. New Trends Nucl. Syst. Thermohydraulics, 467–477.

D'Auria, F., Melikhov, O., Melikhov, V., Elkin, I., Suslov, A., Bykov, M., Del Nevo, A., Araneo, D., Muellner, N., Cherubini, M., 2006. Accident Management Technology in VVER-1000. University of Pisa, Pisa, Italy.

Del Nevo, A., Adorni, M., D'Auria, F., Melikhov, O.I., Elkin, I.V., Schekoldin, V.I., Zakutaev, M.O., Zaitsev, S.I., Benčík, M., 2012. Validation of advanced computer codes for VVER technology: LB-LOCA transient in PSB-VVER facility. Sci. Technol. Nucl. Installations 2012, 15.

Groudev, P.P., Stefanova, A.E., Gencheva, R.V., Pavlova, M.P., 2005. PSB-VVER simulation of Kozloduy NPP "loss of feed water transient". Nucl. Eng. Des. 235, 925–936.

Heralecky, P., 2014. Post-Test Analysis of Upper Plenum 11% Break at PSB-VVER Facility using TRACE V5.0 and RELAP5/MOD3.3 Code (NUREG/IA-0449). U.S. Nuclear Regulatory Commission, Washington, DC.

Kroshilin, A.E., Kroshilin, V.E., Smirnov, A.V., 2006. The application of the BAGIRA code for a computational analysis of accident conditions involving a small leak from the reactor coolant circuit on the PSB-VVER test facility. Therm. Eng. 53, 714–722.

Müllner, N., 2010. Simulation of Beyond Design Basis Accidents: A Contribution to Risk Analysis of Nuclear Power Plants. University of Vienna Austria.

Nevo, A.D., D'Auria, F., Mazzini, M., Bykov, M., Elkin, I.V., Suslov, A., 2008. The design of PSB-VVER experiments relevant to accident management. J. Power Energy Syst. 2, 371–385.

Petruzzi, A., D'Auria, F., 2008. Thermal-hydraulic system codes in nulcear reactor safety and qualification procedures. Sci. Technol. Nucl. Installations 2008.

Prošek, A., D'Auria, F., Mavko, B., 2002. Review of quantitative accuracy assessments with fast Fourier transform based method (FFTBM). Nucl. Eng. Des. 217, 179–206.

Prošek, A., D'Auria, F., Richards, D.J., Mavko, B., 2006. Quantitative assessment of thermal-hydraulic codes used for heavy water reactor calculations. Nucl. Eng. Des. 236, 295–308.

Prošek, A., Kvizda, B., Mavko, B., Kliment, T., 2004. Quantitative assessment of MCP trip transient in a VVER. Nucl. Eng. Des. 227, 85–96.

Prošek, A., Leskovar, M., 2015. Use of FFTBM by signal mirroring for sensitivity study. Ann. Nucl. Energy 76, 253–262.

Prošek, A., Leskovar, M., Mavko, B., 2008. Quantitative assessment with improved fast Fourier transform based method by signal mirroring. Nucl. Eng. Des. 238, 2668–2677.

Saghafi, M., Ghofrani, M., 2015. Introduction of a research project on development of accident management support tool for BNPP (WWER-1000) based on the lessons learned from Fukushima accident. In: International Experts Meeting on Strengthening Research and Development Effectiveness in the Light of the Accident at the Fukushima Daiichi Nuclear Power Plant. Vienna, Austria.

Saghafi, M., Ghofrani, M.B., D'Auria, F., 2016. Development and qualification of a thermal-hydraulic nodalization for modeling station blackout accident in PSB-VVER test facility. Nucl. Eng. Des. 303, 109–121.

Shahedi, S., Jafari, J., Boroushaki, M., D'Auria, F., 2010. Development of a qualified nodalization for small-break LOCA transient analysis in PSB-VVER integral test facility by RELAP5 system code. Nucl. Eng. Des. 240, 3309–3320.